Draft version June 21, 2014
Preprint typeset using LaTeX style emulateapj v. 5/2/11

arXiv:1401.1985v1 [astro-ph.GA] 9 Jan 2014

METALLICITY INHOMOGENEITIES IN LOCAL STAR-FORMING GALAXIES AS SIGN OF RECENT METAL-POOR GAS ACCRETION

J. Sánchez Almeida[1,2], A. B. Morales-Luis[1,2], C. Muñoz-Tuñón[1,2], D. M. Elmegreen[3], B. G. Elmegreen[4], and J. Méndez-Abreu[1,2,5]

Draft version June 21, 2014

ABSTRACT

We measure the oxygen metallicity of the ionized gas along the major axis of seven dwarf star-forming galaxies. Two of them, SDSSJ1647+21 and SDSSJ2238+14, show $\simeq 0.5$ dex metallicity decrements in inner regions with enhanced star-formation activity. This behavior is similar to the metallicity drop observed in a number of local tadpole galaxies by Sánchez Almeida et al., and interpreted as showing early stages of assembling in disk galaxies, with the star formation sustained by external metal-poor gas accretion. The agreement with tadpoles has several implications: (1) it proves that galaxies other than the local tadpoles present the same unusual metallicity pattern. (2) Our metallicity inhomogeneities were inferred using the direct method, thus discarding systematic errors usually attributed to other methods. (3) Taken together with the tadpole data, our findings suggest a threshold around one tenth the solar value for the metallicity drops to show up. Although galaxies with clear metallicity drops are rare, the physical mechanism responsible for them may sustain a significant part of the star-formation activity in the local Universe. We argue that the star-formation dependence of the mass-metallicity relationship, as well as other general properties followed by most local disk galaxies, are naturally interpreted as side effects of pristine gas infall.Alternatives to the metal poor gas accretion are examined too.

Subject headings: galaxies: abundances – galaxies: dwarf – galaxies: evolution – galaxies: formation – galaxies: kinematics and dynamics – galaxies: structure

1. INTRODUCTION

There are two major modes of galaxy formation, as inferred from cosmological numerical simulations (e.g., Silk & Mamon 2012; Dekel & Birnboim 2006). At large redshifts major mergers play the dominant role, where galaxies of similar masses merge to form larger agregates. As the universe evolves, a second mechanism takes over. The proto-galaxies grow by accretion of external flows of pristine gas, that penetrate the dark matter halo and hit and heat a pre-existing elementary disk. Cosmological simulations predict this cold-flow buildup to be the main mode of galaxy formation (Dekel et al. 2009a; Genel et al. 2012), and the incoming gas is expected to form giant clumps that spiral in and merge into a central spheroid (Noguchi 1999; Genzel et al. 2008; Elmegreen et al. 2008), or just create thick disks that evolve by secular processes (Dekel et al. 2009a; Brook et al. 2012).

Observational evidence for this cold-flow accretion mode comes from the decrease of metallicity associated with internal star-formation regions in high redshift disk galaxies (Cresci et al. 2010). Such localized metallicity drops in the inner disk cannot be explained in any other obvious way but the accretion of external metal poor gas – secular evolution produces disks with a metallicity decreasing inside-out (e.g., Vilchez et al. 1988; van der Kruit & Freeman 2011; Moran et al. 2012), in sharp contrast with these observations. The same kind of metallicity deficit associated with bright star-forming regions has also been observed in a particular type of local galaxies with tadpole morphology (Sánchez Almeida et al. 2013b). Their images show a large star-forming clump at one end and a long diffuse region to one side. This asymmetric morphology is fairly common at high redshift (Elmegreen et al. 2007; Elmegreen & Elmegreen 2010; Straughn et al. 2006; Windhorst et al. 2006) but rare in the local Universe (Elmegreen et al. 2012b), where it turns out to be associated with extremely metal poor galaxies, and so, with chemically primitive objects (Papaderos et al. 2008; Morales-Luis et al. 2011; Filho et al. 2013).These facts were used by Elmegreen et al. (2012b) and Sánchez Almeida et al. (2013b) to conjecture that local tadpole galaxies are disks in early stages of assembling. Metallicity drops associated star-forming regions have also been observed in few other local targets, including a gamma ray burst host galaxy (Levesque et al. 2011) and a Blue Compact Dwarf (BCD) galaxy (Werk et al. 2010). They are interpreted in terms of redistribution of centrally generated metals, with strong galactic winds and subsequent fall-back, but not as cold-flow accretion events.

Here we analyze the spatial variation of metallicity in a set of BCD galaxies with intense starbursts and having a range of metallicities from 2/3 to 1/20 the solar value. The purpose of the work is twofold. First, to see whether the metallicity inhomogeneities observed in tadpoles are also present in other local targets different from the orig-

jos@iac.es, abml@iac.es, cmt@iac.es, elmegreen@vassar.edu, bge@us.ibm.com, jmad@st-andrews.ac.uk
[1] Instituto de Astrofísica de Canarias, E-38205 La Laguna, Tenerife, Spain
[2] Departamento de Astrofísica, Universidad de La Laguna, Tenerife, Spain
[3] Department of Physics and Astronomy, Vassar College, Poughkeepsie, NY 12604, USA
[4] IBM Research Division, T.J. Watson Research Center, Yorktown Heights, NY 10598, USA
[5] School of Physics and Astronomy, University of St Andrews, North Haugh, St Andrews, KY16 9SS, UK

inal sample (Sect. 2). Second, and equally relevant, to check if the metallicity variations remain when the metallicities are estimated via the direct method. Thus we can discard a systematic error in the strong-line method employed by Sánchez Almeida et al. (2013b) to infer the abundance inhomogeneities (e.g., Stasińska 2010).

The result of our analysis confirms that, at least in two targets, there are metallicity drops associated with intense starbursts. These drops are not present in the objects of larger metallicity. We use this fact to conjecture that a minimum metallicity around 1/10 the solar value is needed for the metallicity decrements to be observed. Galaxies with metallicities below this one tenth threshold are usually referred to as extremely metal-poor (XMP; e.g., Kunth & Östlin 2000).

One might interpret the rarity of galaxies with metallicity drops as evidence against systematic cold-flow accretion in the local Universe. Thus the few observed decrements would represent vestiges of a physical process common early on, but now almost inoperative. However, several independent observations suggest that star-formation triggered by accretion of metal-poor (perhaps pristine) gas may be a process more common than anticipated. Several of those evidences are put forward and discussed in detail in Section 5, all of them involving global properties of large numbers of galaxies. The most conspicuous one refers to the so-called mass-metallicity relation. It has been recently found (Mannucci et al. 2010; Lara-López et al. 2010; Pérez-Montero et al. 2013; Andrews & Martini 2013) that for galaxies of the same mass, their current star-formation rate (SFR) is anti-correlated with their ionized gas metallicity. No contrived explanation is required if the two parameters are physically connected, as if the infall of metal-poor gas feeds and triggers the star formation in these galaxies (Brisbin & Harwit 2012; Davé et al. 2012).

The paper is organized as follows: Section 2 describes observations and reduction. Metallicity estimates are outlined in Section 2.1. The resulting gradients and inhomogeneities are analyzed in Section 3. Potential observational biases and alternatives to the metal poor gas accretion are examined in Sect. 4. Observational evidences for grand-scale gas inflows triggering star-formation in the local Universe are presented and discussed in Section 5. The implications of our work are considered in Sect. 6.

2. OBSERVATION AND DATA ANALYSIS

The seven galaxies used in this study are listed in Table 1. Even though their spectra were originally obtained with a different purpose[6], they turned out to be ideal for our work. Their long-slit spectra provide spatial resolution within the targets, with a spectral coverage enough to detect all the lines required for oxygen abundance analysis using the direct method. The targets cover a wide range metallicities, from 2/3 to 1/20 the solar metallicity (see Table 1, with $12+\log(\mathrm{O/H})_\odot = 8.69$ as measured by Asplund et al. 2009). In addition, the galaxies form stars actively, in the sense that the current starburst is much larger than the average SFR during the galaxy lifetime (assumed to be similar to the age of Universe t_0, since the galaxies presumedly contain old stellar populations – see, e.g., Papaderos et al. 1996; Corbin et al. 2006; Sánchez Almeida et al. 2012). The time-scale $t_\star$ to produce their stellar masses $\mathrm{M}_\star$ at the current star formation rate (SFR),

$$t_\star = \mathrm{M}_\star/\mathrm{SFR}, \quad (1)$$

is typically much smaller than one Gyr (see Table 1), and so much smaller than t_0 ($\simeq$14 Gyr). The SFRs and stellar masses in Table 1 use SDSS Hα fluxes, colors and magnitudes together with the prescriptions in Kennicutt (1998) and Elmegreen et al. (2012b), and the mass-to-light ratios in Bell & de Jong (2001).

All long-slit spectra were taken with the spectrograph ISIS of the 4.2 m William Hershel Telescope (WHT) operated in the Roque de los Muchachos Observatory[7]. The dual beam, red and blue, covers in a single exposure from λ3600 Å to 8000 Å. The ISIS@WHT setup includes intermediate gratings which, after a 2×2 binning of the CCD, provide 1.7 Å pix^{-1} (blue) and 1.9 Å pix^{-1} (red) equivalent to 0.″40 pix^{-1} (blue) and 0.″44 pix^{-1} (red). We use a slit 1″ wide, which limits the angular resolution, and also sets the spectral resolution to some 4.2 Å both in the red and the blue arms. This resolution suffices to measure the fluxes of the relevant emission lines [OIII]$\lambda\lambda$4363,4959,5007 Å, [OII]$\lambda\lambda$3727,7319,7330 Å, Hβ, Hα, [NII]λ6584 Å, and [SII]$\lambda\lambda$6717,6731 Å. The observations were carried out in two campaigns (Jan 31, 2009, and July 15, 2010), both with fair-to-good seeing from 1.″3 and 0.″5. We integrated 4000 s on target. Some of the objects show an elongated morphology (Table 1), and then the slit was oriented along the major axis. Otherwise, the slit followed the parallactic angle.

The reduction procedure included standard bias and flatfield corrections, cosmic ray elimination, absolute flux calibration, as well as removal of sky emission lines. Spectral and spatial directions were not exactly perpendicular on the CCD, and we also correct for this effect. The spectra were aligned so that each column corresponds to a single position on the sky. Thus the different columns are extracted and analyzed independently in the paper, with each spectrum representing 0.″44 on the galaxy. After these manipulations, the signal-to-noise ratio (S/N) in Hα turns out to be between 1000 and 300 from the center to the outskirts of a typical galaxy. The critical line needed for electron temperature determination, [OIII]λ4363 Å, is much fainter than Hα, but it still reaches a S/N up to 70 in the brighter regions. As we explain below, S/N $\to$ 0 (this line disappears) when the metallicity becomes large. Figure 1 contains an example of one of these fully reduced spectra, specifically, the brightest knot of `J1509+37` (Table 1).

2.1. *Metallicity Determination*

We determine the oxygen abundance using the direct method (e.g., Shaw & Dufour 1995; Stasińska 2004), fol-

[6] Specifically, for checking the metallicity of XMP candidates selected from SDSS/DR6 as BCDs having negligible [NII]λ6583 Å (Sect. 2.2 in Sánchez Almeida et al. 2008). The absence of this line is a signature of low metallicity (e.g., Denicoló et al. 2002; Morales-Luis et al. 2011), but most of the candidates from Sánchez Almeida et al. (2008) lack [NII]λ6583 Å due to an artifact of the reduction pipeline, that removed [NII] together with an overlapping telluric line. Thus they present a range of metallicities.

[7] `http://www.ing.iac.es/astronomy/telescopes/wht/`

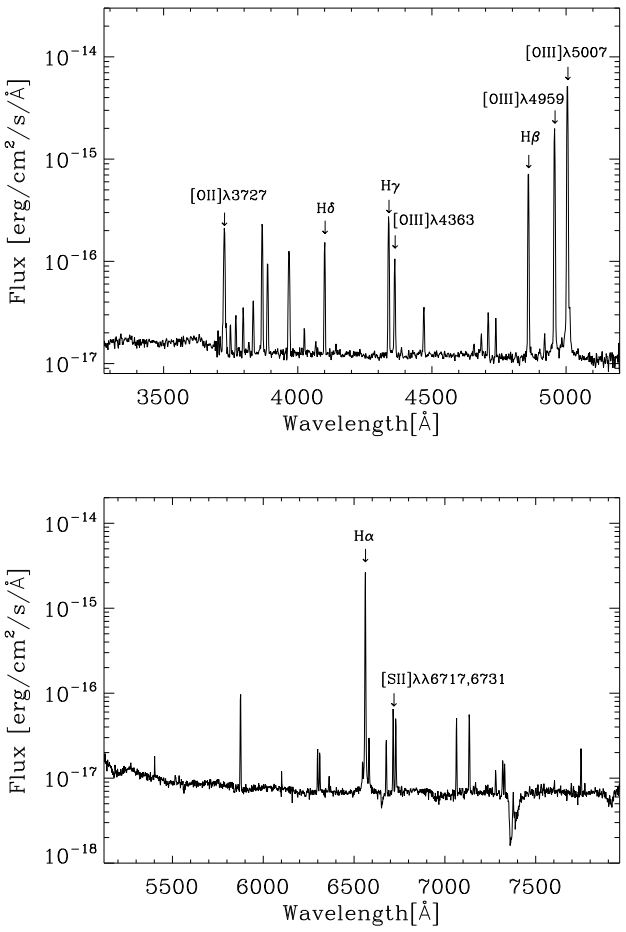

FIG. 1.— Example of one of the spectra used in the work, with the main emission lines included. It corresponds to the brightest knot of J1509+37. The spectra of the two arms of the spectrograph are shown in different panels – the upper and the lower panels correspond the blue and the red arms, respectively. Fluxes are given in a logarithmic scale to show faint lines.

lowing the prescription by Hägele et al. (2008), which includes employing the Balmer decrement to correct for internal reddening. Electron densities were calculated using the ratio of fluxes [SII]λ6717Å/[SII]λ6731Å. The electron temperature of [OIII] was derived from the ratio ([OIII]λ4959Å+[OIII]λ5007Å)/[OIII]λ4363Å. The ratio [OII]λ3727Å/([OII]λ7319Å+[OII]λ7330Å) was used to measure the electron temperature of [OII] or, when this line was not available, calculated using the relationship between [OII] and [OIII] temperatures worked out by Pérez-Montero & Díaz (2003) . We use throughout the manuscript the term *modified direct method* to describe this approach to [OII] temperature estimate. Finally, the oxygen metallicity is computed by adding up the contribution of all oxygen ionization states up to O^{2+}. The errors in the oxygen abundances were computed in a Monte-Carlo simulation, by randomly modifying the fluxes of the emission lines according to the noise of the observed spectra as measured in their continua and scaled up to account for the photon noise (e.g., Pérez-Montero & Díaz 2003, Sect. 3.1). The abundances are computed from 500 realizations of the noise, and the standard deviation of the resulting O/H are quoted as error bar. In a second error estimate, we repeated the Monte-Carlo exercise assuming the noise in continuum to be three times the observed one.

In addition to the direct method, in order to compare it with the metallicities and metallicity variations found by Sánchez Almeida et al. (2013b), we also estimate the oxygen abundance using the ratio [NII]λ6583 Å to Hα. It is the so-called N2-method as proposed by Denicoló et al. (2002), and we use it in the calibration by Pérez-Montero & Contini (2009).

3. SPATIAL VARIATION OF METALLICITY

The direct-method based oxygen abundance corresponding to the spatially integrated spectra of all the observed galaxies is given in Table 1. They represent the luminosity-weighted average metallicity. Even though all targets are metal-poor, only J2238+14 is XMP in the usual sense of having an average metallicity smaller than a tenth of the solar value (i.e., $12 + \log(\mathrm{O/H}) \leq 7.69$; Asplund et al. 2009, and Section 1).

Figures 2, 3 and 4 show the three types of observed spatial variations. The Sloan Digital Sky Survey (SDSS Stoughton et al. 2002; Ahn et al. 2012) images on top indicate the orientation of the slit. The bottom panels plot oxygen abundance versus position along the slit in arcsec, using as reference position the pixel of largest Hα flux. Abundances inferred from the direct method are represented as black dots joined by black solid lines. These are the measurements we discuss unless otherwise stated. Abundances from the modified direct method (the blue lines) and N2 (the red lines) are analyzed later on. The targets J0942+34, J2302+00 behave similarly, the latter represented in Fig. 2, in the sense that the spatial region with enough S/N to carry out the metallicity measurement is too small to provide any reliable spatial variation. Seeing during observation was of the order of $1''$ (Sect. 2), which is similar to the spatial extent of the signals on the CCDs (see the continuum and Hα fluxes in Fig. 2, represented as the orange and green histograms, respectively). Figure 3, the black solid line, shows a rather constant metallicity, and this time the galaxy is significantly larger than the seeing. The figure displays J1509+37, but its behavior also stands for J1003+45. These galaxies show no obvious metallicity gradient or drop. Finally, Fig. 4 portrays J2238+14 which clearly shows two metallicity decrements associated with the two bright knots of the galaxy – compare the black solid line representing O/H with the Hα and continuum fluxes shown as histograms. The metallicity drop corresponds to $\Delta[12 + \log(\mathrm{O/H})] \simeq -0.5$. J2238+14 is the galaxy of lowest average metallicity in the sample (see the dashed line corresponding to $\mathrm{O/H} = (\mathrm{O/H})_\odot/10$, which is common to the three figures). Figure 5 is similar to Fig. 4 in the sense of showing a significant spatial variation of metallicity for J1647+21. The source is larger and more complex than J2238+14 (Fig. 5). The long slit spectrum has not enough signal for metallicity analysis in between the two main galaxy knots (except for a single pixel in between; see Fig. 5). However, the signals in the knots clearly indicate a significant difference of metallicity. The brightest one (at position zero) has a metallicity of the order of 1/10 solar, whereas the second

TABLE 1
Global parameters of the galaxies

Name[a]	$12+\log(O/H)$[b]	g[c]	$\log M_\star$[d] $[M_\odot]$	SFR[e] $[M_\odot yr^{-1}]$	$M_\star/SFR$[f] [Gyr]	Redshift $\times 10^2$	Morphology	$\Delta \log(O/H)$?
SDSSJ083713.13+360350.4	8.54 ± 0.01	17.4	9.14	0.68	2.0	3.31	single knot	no
SDSSJ094254.27+340411.8	7.79 ± 0.05	19.1	7.34	0.33	0.068	2.25	single knot	unclear
SDSSJ100348.65+450457.7	7.89 ± 0.01	17.6	7.60	0.15	0.27	0.92	single knot	no
SDSSJ150934.17+373146.1	7.80 ± 0.01	17.3	7.51	3.62	0.009	3.25	cometary	no
SDSSJ164710.66+210514.5	8.11 ± 0.03	16.9	7.73	0.43	0.12	0.91	cometary	yes
SDSSJ223831.12+140029.7	7.43 ± 0.01	18.7	7.55	0.51	0.070	2.06	two-knots	yes
SDSSJ230210.00+004938.8	7.75 ± 0.03	18.8	7.27	0.75	0.025	3.31	two-knots	unclear

[a] Named so that right ascension and declination are implicit.
[b] From the spatially integrated spectrum.
[c] Integrated g magnitude provided by SDSS/DR9.
[d] Masses from SDSS/DR9 photometry using mass-to-light ratios by Bell & de Jong (2001).
[e] Star Formation Rate from Hα flux using the prescription in Elmegreen et al. (2012b).
[f] Time to form all stars in the galaxy at the current SFR – inverse specific SFR.

one (at positions between $-35''$and $-40''$) is doubtless metal richer, even though we cannot assess its actual metallicity. The spectrum in the metal-rich knot does not show [OIII]λ4363 Å, needed for electron temperature estimates. However, this lack implies a low electron temperature, and so a high metallicity – McGaugh (1991); Sánchez Almeida et al. (2012). We estimate a lower limit of $12+\log(O/H) \geq 8.2$ computing the metallicity with a [OIII]λ4363 Å flux just below the continuum noise level in our spectra. This lower limit is represented in Fig. 5.

Table 1 contains a flag indicating whether the metallicity variations are present in the galaxies, are not present, or are unclear. It is unclear in the two galaxies that are too small. Discarding them, 40% of the galaxies show metallicity drops (two out of five objects).

Figures 2, 3, 4 and 5 include metallicities derived from the semi-empirical N2 method (the blue dots joined by blue solid lines). Overall, they show the same trends and drops as the direct method confirming that at least for these targets both techniques provide qualitatively consistent results. In some cases there are small differences, e.g., the drop of N2 metallicity in `J1509+37`, which is not obvious in the direct method based metallicity (Fig. 3). However, these discrepancies are within the 0.2 dex scatter typical of the N2 calibration (e.g., Pettini & Pagel 2004; Pérez-Montero & Contini 2009). This is more clear in Fig. 3 where the error bars include both the noise in the spectra plus 0.2 dex ascribed to the N2 calibration. The figures also include oxygen abundances inferred from the alternative direct method (Sect. 2.1), and they also agree with the rest (see the red solid lines in the figures). The error bars propagated from the noise in the spectra (Sect. 2.1) are unrealistically small for reasons that we ascribed to bias in the flux estimates not accounted for when propagating the continuum error. In order to make them more realistic, errors were computed also increasing the observed continuum noise by a factor of three. These other larger error bars are only represented in Fig. 3.

The galaxy `J0837+36` has not been mentioned so far because its case slightly differs from the rest. It is more massive and with lower specific SFR (i.e., SFR/$M_\star$; Table 1). Its metallicity is so large that [OIII]λ4363 Å is not detectable in individual spatial pixels and so, direct-method metallicity gradients cannot be computed. As we explained above for the high metallicity knot of `J1647+21`, the absence of this line proves the high metallicity of the HII gas, even though we cannot quantify it. From the N2-based estimate, we conclude that the metallicity variations of this galaxy are negligible small, as indicated in the last column of Table 1.

4. ALTERNATIVES TO THE INFERRED METALLICITY DECREMENTS

This section analyzes alternatives to explaining the observed metallicity drops as the outcome of a metal-poor gas accretion event. Specifically, we point out possible biases of the direct method that artificially produce low metallicities (Sect. 2.1), as well as a mechanism that may lead to the metal impoverishment of regions with long-lasting intense starbursts. Even though these potential problems cannot be fully ruled out, accretion of pristine gas remains to be the simplest way of explaining the observations.

If the temperature in the region is not homogeneous, then the direct method underestimates the true abundances (Peimbert 1967; Peimbert & Costero 1969). There is a long-lasting debate in the literature on whether such temperature fluctuation exists (Stasińska et al. 2013, and references therein). An artificial reduction of metallicity of 0.5 dex can be produced by temperature fluctuations of the order of 20-30% rms (e.g., Stasińska 2004; Esteban et al. 2009). If this effect is responsible for the observed drop of metallicity, then such fluctuations should be localized in the low metallicity starburst, but not in the rest of the galaxy. We cannot rule out this possibility since the interstellar medium (ISM) of our targets is poorly known. We note, however, that the physical mechanisms proposed to generate temperature inhomogeneities favor high metallicity media rather than our XMP galaxies (see the review by Torres-Peimbert & Peimbert 2003). For example, they require dust particles for heating (e.g., Stasińska & Szczerba 2001), or they need metals for the metallicity inhomogeneities to cause the temperature fluctuations (e.g., Kingdon & Ferland 1998).

The direct method does not consider the presence of density fluctuations, which in some real cases may be large. The resulting electron density variations are not expected to have significant impact on the abundances (e.g., Stasińska et al. 2012), however, density inhomogeneities may have an indirect influ-

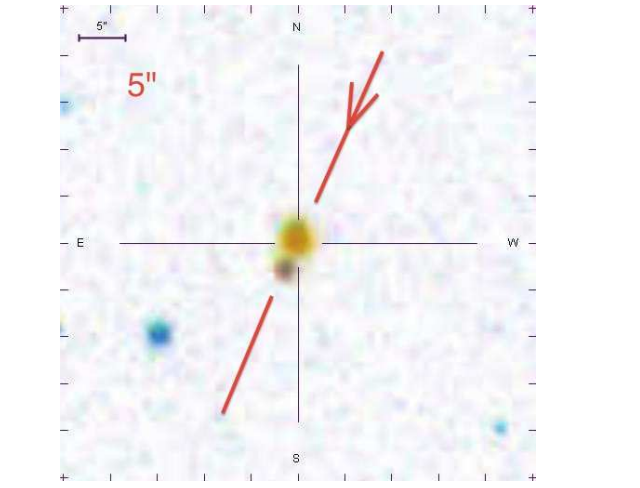

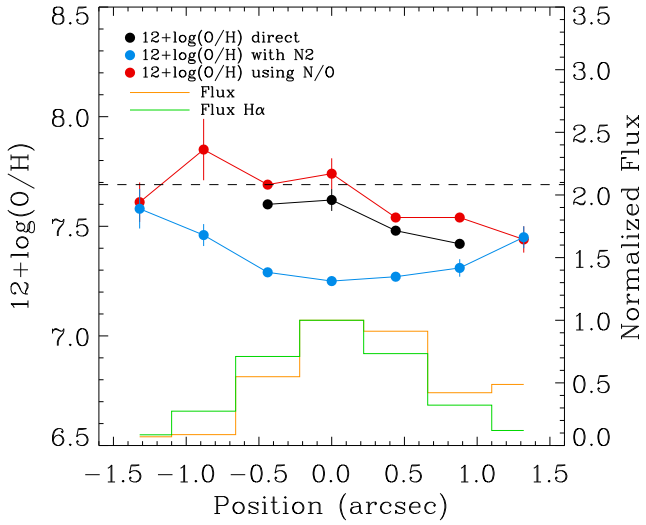

FIG. 2.— Top: color-code inverted SDSS image of the galaxy J2302+00. The red line indicates the orientation of the spectrograph slit, with the arrow pointing in the sense of growing position along the slit. The scale corresponds to 5″on the sky. Bottom: metallicity and flux variation along the slit of this target. We show the metallicity computed using the direct method (the black solid line joining black points), the modified direct method described in Sect. 2.1 (the red solid line), and the N2 method (the blue solid line). The flux of the integrated spectrum and the Hα flux are given as orange and green histograms, respectively. Their values have been normalized to the largest flux, and the ordinate axis on the right-hand-side of the plot refers to them. The scale of oxygen metallicity is given on the left-hand-side of the plot. Positions along the slit are in arcsec refereed to the point of largest Hα flux. In this particular target only the main galaxy knot is detected. The extent is too small as compared to seeing to decide whether there are significant variations of metallicity. The dashed line indicates a tenth of the solar metallicity, a line used for reference. The error bars account only for random noise in the observed spectra. Other sources of error are included in Fig. 3.

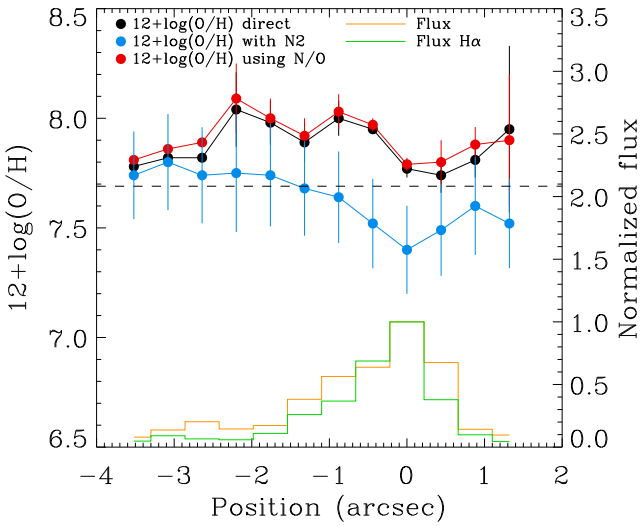

FIG. 3.— Same as Fig. 2 but corresponding to the target J1509+37. This time the spectral signals extend over a region larger than the seeing and so we detect no obvious metallicity variation along the slit. For the meaning of the various axes, curves and symbols, see Fig. 2. The dashed line corresponds to 1/10 of the solar metallicity. The continuum noise has been artificially increased by a factor of three to compute the error bars in this plot. In addition, the N2 abundance errors have been enlarged by 0.2 dex to include the scatter of the N2 metallicity calibration.

ence though induced temperature inhomogeneities (e.g., Torres-Peimbert & Peimbert 2003). If the plasma is heated by collisions with photo-ionized electrons, dense clumps present lower temperatures, leading to temperature fluctuations. Detailed tailored modeling is required to assess the practical importance of the effect. If it is meant to explain the observed metallicity drops, the largest density fluctuations must occur where the metallicity appears to be lowest.

In order to determine the oxygen abundance, the standard direct method used in the paper includes only O, O^+ and O^{2+}, but not higher ionization states. Since the ionizing radiation field is harder in young star-forming regions, one may wonder whether our metallicity drops are actually caused by overlooking O^{3+} in large starbursts. However, this potential bias does not explain the magnitude of the observed drops. Even when very hot stars are present in HII regions, the correction for unseen states of oxygen is negligible small with respect to other sources of errors (e.g., Stasińska et al. 2012). The ionization correction factors for O^{3+} are never of the order of 0.5 dex as required to reproduce our observations (e.g., Kingsburgh & Barlow 1994).

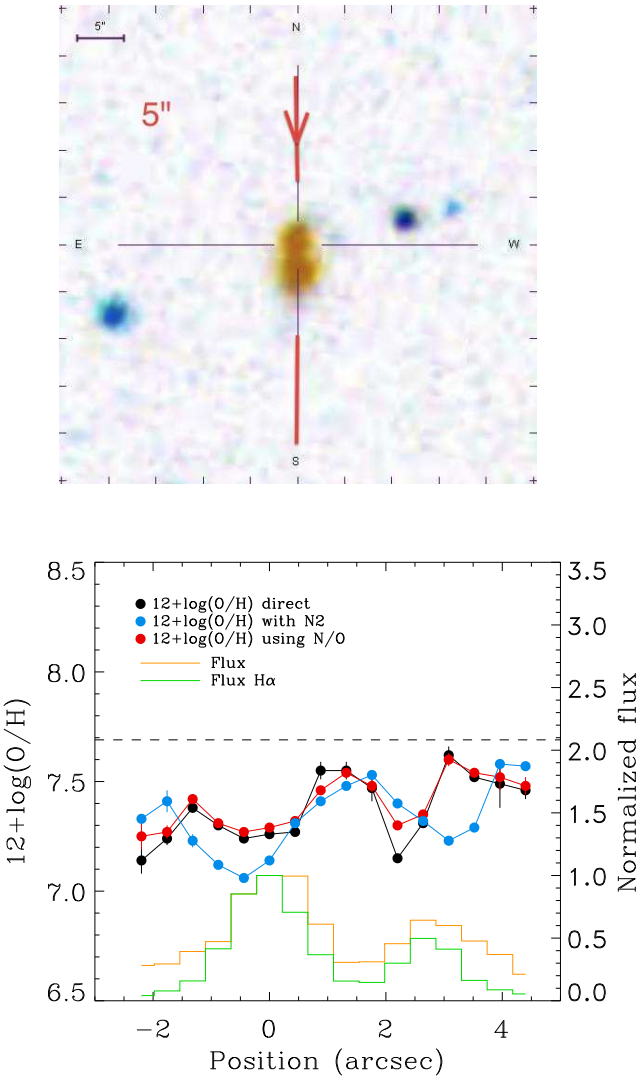

FIG. 4.— Same as Fig. 2 but corresponding to J2238+14. The target is larger than the seeing, and it shows a clear metallicity variation along the slit (the black solid line) with a pattern similar to the Hα flux variation (the green histogram). For the meaning of the other curves and symbols, see Fig. 2. The dashed line corresponds to 1/10 of the solar metallicity. The error bars account only for random noise in the observed spectra. Other sources of error are included in Fig. 3.

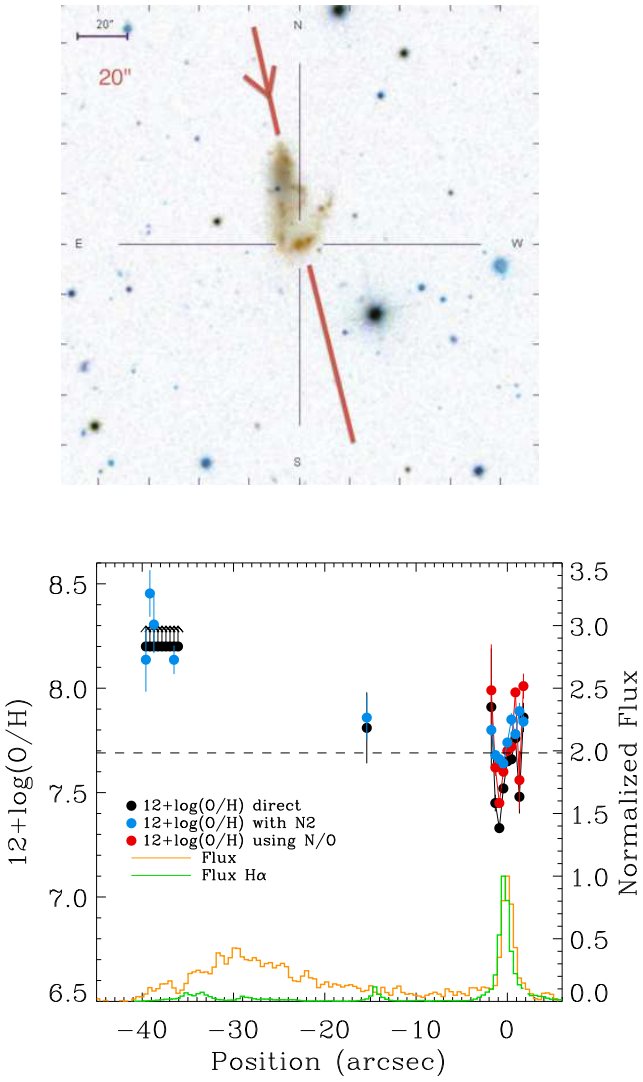

FIG. 5.— Same as Fig. 2 but corresponding to J1647+21 The galaxy is larger than the seeing, and it shows metallicity variations along the slit (the black dots), with a pattern similar similar to the Hα flux variation (the green histograms). For the meaning of the other curves and symbols, see Fig. 2. The zero of the position scale in the bottom plot corresponds to the center of the large cross in the upper image. Positions along the slit grow in the sense indicated by the arrow on the top image. The error bars account only for random noise in the observed spectra. Other sources of error are included in Fig. 3.

Dwarf galaxies have shallow gravitational potentials that cannot retain all the metals ejected by SNa explosions (e.g., Mac Low & Ferrara 1999). Therefore, their metal enrichment depends critically on two competing processes, both controlled by the SNa rate, that is to say, controlled by the SFR – the metal production and the metal loss. Both increase with the SFR. Due to this interplay, dwarfs may enrich more efficiently at mild SFRs, where the two opposite effects reach a compromise (Hidalgo et al. 2011; Koleva et al. 2013). This trade-off between SFR and metallicity may induce the metallicity pattern that we observe. If a major starburst has been losing most of the metals for long, the gas around it would have a metallicity lower than the rest of the galaxy, where the star-formation has proceeded at a lower more-efficient rate. Even though we cannot fully discard this possibility, we envisage two difficulties for this explanation to work with our targets. First, the high star-formation mode quickly exhausts the original gas supply, which has to be replenished with metal poor gas that does not exist in the galaxy. Second, and equally important, the gas in the star-bursting region should remain unmixed or the full galaxy would acquire a uniform metallicity. This is not easy to attain since mixing mechanisms are expected to efficiently operate in short time-scales (Myrs; e.g., Tenorio-Tagle 1996; de Avillez & Mac Low 2002).

5. UBIQUITY OF THE PHENOMENON

A number of observational properties characterizing large samples of star-forming galaxies can be naturally explained if the metallicity drop associated with intense

starbursts is a common phenomenon. The inflow of pristine gas provides a simple physical unifying mechanism that explains all of them, even though often it is not the only explanation of each individual observation. This section critically reviews some of these results in terms of metal-poor gas inflow triggering star-formation. The discussions are fairly qualitative, emphasizing the diversity of observations hinting at grand-scale metal-poor gas inflows in the local galaxies.

5.1. *The mass-metallicity-starformation-rate relationship*[8]

Local galaxies are known to follow a mass-metallicity relationship, where the larger the mass the higher the metallicity (e.g., Skillman et al. 1989; Tremonti et al. 2004; Gallazzi et al. 2005). The relationship presents a significant scatter that has been recently found to be associated with the present SFR in the galaxy (Mannucci et al. 2010; Lara-López et al. 2010; Yates et al. 2012; Pérez-Montero et al. 2013; Andrews & Martini 2013; Zahid et al. 2013). Specifically, for galaxies with the same stellar mass, the metallicity decreases as the current SFR increases. The mass-metallicity relationship is commonly interpreted as due to variations of the star-formation efficiency with galaxy mass, and/or to galaxy mass-dependent metal-rich outflows (e.g., Lee et al. 2008; Ellison et al. 2008). The former implies that low mass galaxies produce less stars for their gas, and so become more metal poor, whereas the latter relies on the metal-rich SNa ejecta to be preferentially lost to the intergalactic medium by low mass galaxies, due to their shallower gravitational well. Neither of these two mechanisms, however, predict the observed dependence on SFR of the metallicity – they render a metallicity set only by the galaxy mass[9]. Conversely, the observed anti-correlation between metallicity and SFR can be qualitatively understood if the star-formation is preferentially triggered and sustained by the inflow of metal-poor gas, which has no time to be well mixed with the high metallicity gas already present in the ISM of the galaxies. The agreement is more than qualitative according to Brisbin & Harwit (2012). Using a toy model for the gas inflow, these authors conclude that most of the star-forming galaxies with stellar masses $M_\star \leq 2 \times 10^{10}\,\mathrm{M}_\odot$, and many with $M_\star \geq 2 \times 10^{10}\,\mathrm{M}_\odot$ appear to be fed by low-metallicity gas infall. The importance of metal-poor gas infall to account for the observed mass-metallicity-SFR relationship is also emphasized by Davé et al. (2012) and Dayal et al. (2013) in their simple analytic chemical evolution models that include mass infall and outflows. In particular, Davé et al. (2012) explain the metallicity-SFR relationship as transient departures from the secular evolution of the galaxies, triggered by sudden infalls of metal-poor gas.

Unlike the metallicity, the ratio between the observed N and O does not seem to depend on SFR (see Pérez-Montero et al. 2013; Andrews & Martini 2013). This lack of SFR-dependence is consistent with the relation between metallicity and SFR being maintained by episodic metal-poor inflows. The advent of fresh gas triggers star formation and drops the metallicity, but it does not change the pre-existing relative abundance between metals.

The mass-metallicity- SFR relationship is followed by large numbers of star-forming galaxies so it represents a behavior common to the typical galaxies of the local Universe. It is not restricted to a few rare vestigial objects. Therefore, if the above conjecture turns out to be correct, and pristine gas infall is responsible for the SFR dependence, then this infall is a characteristic of the full population of local star-forming galaxies. This conclusion is the central point of the section.

5.2. *High metallicity of quiescent BCDs*

BCD galaxies are high surface brightness targets and thus, relatively easy to detect. Most XMPs are also BCDs (e.g., Kunth & Östlin 2000; Morales-Luis et al. 2011). The luminosity of these galaxies is dominated by one or several young starbursts, however, most if not all BCDs contain host galaxies with old stars (e.g., Papaderos et al. 1996; Cairós et al. 2003; Corbin et al. 2006; Amorín et al. 2007). The dominant starburst is so intense that it cannot be sustained for long, therefore, the BCDs have to be in a transient phase. (Using the arguments and symbols in Sect. 2, their $t_\star << t_0$.) Consequently, there must be many local galaxies in the pre or post BCD phase, i.e., many quiescent BCDs (or, for short, QBCDs).

The BCD hosts show up in the galaxy outskirts, therefore, deep photometry allowed Amorín et al. (2007, 2009) to characterize their photometric properties. Using the typical host colors and magnitudes as proxies for QBCD properties, Sánchez Almeida et al. (2008) searched the SDSS/DR6 archive for QBCD candidates. They turned out to be rather common – one out of three local dwarf galaxies is of this kind, and there are some thirty of them per BCD galaxy. Their main properties, including their luminosity functions, are consistent with the BCDs being QBCDs observed during a starburst phase in a duty cycle where the QBCD phase lasts 30 times longer than the BCD phase. This interpretation presents a difficulty, though: the gas-phase metallicity of the QBCDs is systematically higher than the metallicity of the BCDs. This cannot happen in a closed-box evolution, where the precursor galaxy always has lower metallicity than the follower, so that QBCDs could not be precursors of BCDs. The problem naturally disappears if almost *every* BCD starburst is preceded by the advent of fresh metal-poor gas that triggers the star formation episode. Moreover, such gas-infall hypothesis beautifully explains why the *stellar* metallicities of BCDs and QBCDs agree, even though their *gas-phase* metallicities do not (Sánchez Almeida et al. 2009). The stars of BCDs and QBCDs are statistically the same because only a small fraction of galaxy stellar mass is produced in each starburst[10]. Their gas differs because BCDs have just rejuvenated their ISM.

[8] Often referred to as *fundamental* mass-metallicity relationship (Mannucci et al. 2010).

[9] At least in simple chemical evolution models. Even if the outflow rate scales with the SFR, the metallicity of the gas is set by the gas fraction, but this gas fraction depends only on the stellar mass (e.g., Edmunds 1990). Thus, given the stellar mass, the metallicity is fixed, leaving no room for a SFR–metallicity correlation.

[10] Although in some extreme cases the present burst may be producing a significant fraction of the stellar mass, e.g., our J1509+37, this is not the general behavior.

This behavior affects not just a few objects, but 30 % of all local dwarfs. Therefore the gas-infall must be a common phenomenon if it is responsible for the metallicity discrepancy between BCDs and QBCDs.

5.3. *The morphology metallicity relationship*

XMP galaxies tend have cometary or other non-symmetric morphologies (Papaderos et al. 2008; Morales-Luis et al. 2011; Filho et al. 2013).Even if surprising, such association seems to be the extreme case of a common relationship between morphology and metallicity followed by the bulk of the star-forming galaxies in the local Universe. Reichard et al. (2009) parameterize lopsidedness in a sample of $\simeq 2.5 \times 10^4$ nearby galaxies, and find that at fixed mass, the more metal-poor galaxies are more lopsided. Whatever process causes lopsidedness, it it is also associated with low metallicity gas in the galaxies. In the case of the XMP, the lopsidedness is produced by off-center large HII regions, fed by pristine gas accretion either directly or indirectly – directly if the gas arrives to the disk ready to form stars (e.g., Dekel et al. 2009a,b), or indirectly if the gas is accumulated until disk instabilities trigger star-formation in regions that must be necessarily large compared to the disk extension (e.g., Noguchi 1999; Elmegreen et al. 2008, 2012a). Low metallicity and lopsidedness come together naturally in XMPs. If the physical mechanism that gives rise to the cometary shape of XMPs is also responsible for the correlation between morphology and metallicity found by Reichard et al. (2009, as an Occam's razor type of argument suggests), then triggering star formation by gas inflow must be quite common.

5.4. *Nitrogen and Oxygen in green-pea galaxies*

Green peas (GPs) are star-forming galaxies which receive this name because of their compactness and green color in SDSS composite images (Cardamone et al. 2009). The color is produced by an unusually large [OIII]λ5007 Å emission line redshifted so as to contribute to the g-band color. They have some of the highest specific SFRs seen in the local Universe, able to double their stellar masses in a fraction of Gyr. GPs seem to be high-mass versions of the most extreme starbursting BCDs (e.g., Izotov et al. 2011; Amorín et al. 2012a), and are low metallicity outliers of the mass metallicity relationship (Amorín et al. 2010, 2012a). Detailed analysis of their emission lines reveals complex kinematical structures with several components coexisting in only a few kpc, which are best interpreted as massive star-forming clumps in a dynamically young host galaxy (Amorín et al. 2012b). Even though GPs have low O metallicity, they present an overabundance of N/O(≥ -1), which is typical of aging stellar populations. This puzzling observation is naturally explained if GPs have recently received a major flood of low metallicity gas (Amorín et al. 2010, 2012a) – the mixing with metal poor gas reduces the metallicity (i.e., O/H), but the ratio between metal species (N/O) remains as in the original high metallicity ISM.

Again, GPs are not special but just extreme cases in the continuous sequence of local star-forming galaxies (e.g., Izotov et al. 2011; Sánchez Almeida et al. 2013a).

5.5. *Other hints of gas accretion*

The literature contains other results that are also suggestive of star-formation triggered by gas accretion at a grand-scale. Some of them are mentioned below.

The neutral gas distribution of the BCD galaxies often shows large distortions, with plumes and tails, and other evidences of gas inflow or outflow (e.g., Brinks & Klein 1988; Wilcots & Miller 1998; Lelli et al. 2012; López-Sánchez et al. 2012; Ashley et al. 2013). Such complex HI morphology appears even in the case of isolated galaxies without obvious companions (Ekta & Chengalur 2010). The distorted gas around BCDs has all signs of having extremely low metallicity, uncontaminated by the ongoing star-formation process (e.g. Lebouteiller et al. 2013; Filho et al. 2013),which suggests that the gas is arriving rather than being expelled from the galaxy.

Even large nearby spirals show local metallicity inhomogeneities that deviate from the main gradient, e.g., M101 (Li et al. 2013). The existence of inhomogeneities is in tension with theoretical expectations, which predict a virtually uniform distribution as a result of the short mixing timescales of the interstellar medium, on the order of only 100 Myr (e.g., Roy & Kunth 1995; Tenorio-Tagle 1996; de Avillez & Mac Low 2002). Localized infall of metal-poor gas may be a viable alternative that explains this particular observation.

As we pointed out in connection with BCDs and GPs (Sects. 5.2 and 5.4), the gas inflow produces large excursions of a galaxy in the N/O vs O/H plane. Numerical models by Köppen & Hensler (2005) allow to explain the observed distribution in irregular and spiral galaxies, but, in order to reach the required large excursions, the mass of the infall gas must be much larger than the mass of the gas present in the galaxy, with the infall rate exceeding the SFR.

This trend for the low metallicity galaxies to show anomalous metallicity gradients (Sect. 3) is also observed at high-redshift (e.g., the z=1.2 MASSIV galaxies; Queyrel et al. 2012). and in several low redshift targets (e.g., Levesque et al. 2011; Werk et al. 2010). The metal-poor galaxies tend to show a positive gradient, whereas metal-rich ones tend to show the negative one expected from secular evolution. Positive gradients naturally arise even from underlying negative gradients when metal-poor gas reaches the central regions of the disks.

6. DISCUSSION AND CONCLUSIONS

We measure the oxygen metallicity along the major axis of seven star-forming dwarf galaxies using different methods, including the direct method (Sect. 2.1; Table 1). Two of them, `J1647+21` and `J2238+14`, show drops of metallicity ($\simeq$0.5 dex) associated with enhanced star-formation activity in central regions. Disk galaxies usually present a negative gradient, with the metallicity decreasing inside out. Therefore, a deficit of metallicity in the inner galaxy is strange, and attributed to the recent arrival of external metal-poor gas that has not yet mixed up with the pre-existing ISM (Sect. 1; other alternatives are also examined in Sect. 4). For this to happen, the incoming gas has to arrive in localized clumps rather than as an isotropic galaxy-wide accretion event. This is the explanation we suggest for the metallicity and Hα

variations observed in J2238+14 (Fig. 4), and J1647+21 too (Fig. 5). The image of the latter, however, may also suggest a merger event, with the main starburst at the collision point (see Fig. 5, with the two colliding disks seen edge-on forming a V-shape in a contrived but not impossible geometry). One of the galaxies would have to be metal-poor gas-rich, with its gas feeding the low metallicity starburst. Actually, such a gas-rich minor merger can also be regarded as a cold-flow accretion event where the accreted gas stream is forming stars along the way (see Dekel et al. 2009a). The different morphology of J2238+14 and J1647+21 may be due to differences in spatial resolution, so that we have a coarser view of the former. But we cannot discard that they reflect qualitative differences in the physical process responsible for the metallicity drops.

Our interpretation of the metallicity drops of J1647+21 and J2238+14 agrees with that given by Sánchez Almeida et al. (2013b) to explain the behavior observed in a number of local tadpole galaxies. Such agreement has several implications. It proves that galaxies other than the sample of tadpole galaxies (Miyauchi-Isobe et al. 2010; Elmegreen et al. 2012b) present the same unusual spatial metallicity pattern. The metallicity inhomogeneities of our targets were inferred using the direct method, which discards the systematic errors usually attributed to strong-line methods (e.g., Shi et al. 2005; Pérez-Montero & Contini 2009). This source of error is discarded for J1647+21 and J2238+14, thus supporting the type of metallicity pattern disclosed in tadpoles (Sánchez Almeida et al. 2013b). Finally, the targets showing the drops tend to have a minimum metallicity smaller than a tenth of the solar value. Something similar happens with the tadpoles analyzed by Sánchez Almeida et al. (2013b), which may suggest a tenth of the solar metallicity to be an observational threshold for the metallicity drops to clearly show up. The origin of the threshold is unclear, but it may reveal an observational bias reflexing the degree of mixing of the galaxy gas. Assume that all typical disks have similar fairly high gas metallicity, and they receive a parcel of metal poor gas. Those galaxies that mix up this metal poor gas with the pre-existing ISM before star-bursting will appear as metal rich targets of homogeneous metallicity. On the contrary, those that produce stars before mixing will look like metal poor galaxies in integrated light, presenting large metallicity inhomogeneities. The actual threshold is probably not universal since high redshift galaxies with drops have metallicities above the one tenth line (Cresci et al. 2010).

If external metal poor gas accretion feeds and triggers star formation, one would expect some kind of kinematical differences between the star-forming clumps and the underlying galaxy disk. These kinematical disturbances are predicted in numerical simulations of minor mergers and cold-flow accretion (e.g., Immeli et al. 2004; Dekel et al. 2009b; Ceverino et al. 2010), and should be sought in real galaxies. Some of then may have been observed already as, e.g., the counter-rotating head found in one of the tadpole galaxies analyzed by Sánchez Almeida et al. (2013b).

Large metallicity inhomogeneities evidence a star formation driven, or at least stimulated, by pristine gas accretion. Even though the number of local galaxies showing inner metallicity inhomogeneities is still limited, there are a number of indirect hints suggesting that metal-poor gas accretion may be more than just a vestige of the early Universe. The argument relies on the existence of general rules or laws followed by large numbers of galaxies, that are naturally explained as star-formation triggered by recent pristine gas infall. It is not the only explanation, but the inflow of pristine gas provides a simple unifying physical mechanism that explain all of them. These evidences are outlined in Sect. 5: among others, the star-formation dependence of the metallicity (Sect. 5.1), the star-formation dependence of the morphology (Sect. 5.3), the high metallicity of quiescent BCDs (Sect. 5.2), and the high N to O ratio in green pea galaxies (Sect. 5.4).

Thanks are due to R. Amorín and E. Pérez-Montero for enlightenning discussions on the constraints on galaxy evolution provided by the observable N/O, to V. Luridiana and M. Koleva for clarifying some of the biases of the direct method, and to J. A. L. Aguerri for technical support during the observing campaigns. Thanks are also due an anonymous referee for helping us sharpening some of the arguments in the paper. This work has been partly funded by the Spanish Ministry for Science, project AYA 2010-21887-C04-04. JMA acknowledges support from the European Research Council Starting Grant (SEDmorph; P.I. V. Wild). The article is based on observations made with the telescope WHT operated at the Spanish *Observatorio del Roque de los Muchachos* of the Instituto de Astrofísica de Canarias.

REFERENCES

Ahn, C. P., Alexandroff, R., Allende Prieto, C., et al. 2012, ApJS, 203, 21
Amorín, R., Aguerri, J. A. L., Muñoz-Tuñón, C., & Cairós, L. M. 2009, A&A, 501, 75
Amorín, R., Pérez-Montero, E., Vílchez, J. M., & Papaderos, P. 2012a, ApJ, 749, 185
Amorín, R., Vílchez, J. M., Hägele, G. F., et al. 2012b, ApJ, 754, L22
Amorín, R. O., Muñoz-Tuñón, C., Aguerri, J. A. L., Cairós, L. M., & Caon, N. 2007, A&A, 467, 541
Amorín, R. O., Pérez-Montero, E., & Vílchez, J. M. 2010, ApJ, 715, L128
Andrews, B. H. & Martini, P. 2013, ApJ, 765, 140
Ashley, T., Simpson, C. E., & Elmegreen, B. G. 2013, AJ, 146, 42
Asplund, M., Grevesse, N., Sauval, A. J., & Scott, P. 2009, ARA&A, 47, 481
Bell, E. F. & de Jong, R. S. 2001, ApJ, 550, 212
Brinks, E. & Klein, U. 1988, MNRAS, 231, 63P
Brisbin, D. & Harwit, M. 2012, ApJ, 750, 142
Brook, C. B., Stinson, G. S., Gibson, B. K., et al. 2012, MNRAS, 426, 690
Cairós, L. M., Caon, N., Papaderos, P., et al. 2003, ApJ, 593, 312
Cardamone, C., Schawinski, K., Sarzi, M., et al. 2009, MNRAS, 399, 1191
Ceverino, D., Dekel, A., & Bournaud, F. 2010, MNRAS, 404, 2151
Corbin, M. R., Vacca, W. D., Cid Fernandes, R., et al. 2006, ApJ, 651, 861
Cresci, G., Mannucci, F., Maiolino, R., et al. 2010, Nature, 467, 811
Davé, R., Finlator, K., & Oppenheimer, B. D. 2012, MNRAS, 421, 98
Dayal, P., Ferrara, A., & Dunlop, J. S. 2013, MNRAS, 430, 2891
de Avillez, M. A. & Mac Low, M.-M. 2002, ApJ, 581, 1047
Dekel, A. & Birnboim, Y. 2006, MNRAS, 368, 2
Dekel, A., Birnboim, Y., Engel, G., et al. 2009a, Nature, 457, 451
Dekel, A., Sari, R., & Ceverino, D. 2009b, ApJ, 703, 785

Denicoló, G., Terlevich, R., & Terlevich, E. 2002, MNRAS, 330, 69
Edmunds, M. G. 1990, MNRAS, 246, 678
Ekta, B. & Chengalur, J. N. 2010, MNRAS, 403, 295
Ellison, S. L., Patton, D. R., Simard, L., & McConnachie, A. W. 2008, ApJ, 672, L107
Elmegreen, B. G., Bournaud, F., & Elmegreen, D. M. 2008, ApJ, 688, 67
Elmegreen, B. G. & Elmegreen, D. M. 2010, ApJ, 722, 1895
Elmegreen, B. G., Zhang, H.-X., & Hunter, D. A. 2012a, ApJ, 747, 105
Elmegreen, D. M., Elmegreen, B. G., Ravindranath, S., & Coe, D. A. 2007, ApJ, 658, 763
Elmegreen, D. M., Elmegreen, B. G., Sánchez Almeida, J., et al. 2012b, ApJ, 750, 95
Esteban, C., Bresolin, F., Peimbert, M., et al. 2009, ApJ, 700, 654
Filho, M. E., Winkel, B., Sánchez Almeida, J., et al. 2013, A&A, 558, A18
Gallazzi, A., Charlot, S., Brinchmann, J., White, S. D. M., & Tremonti, C. A. 2005, MNRAS, 362, 41
Genel, S., Naab, T., Genzel, R., et al. 2012, ApJ, 745, 11
Genzel, R., Burkert, A., Bouché, N., et al. 2008, ApJ, 687, 59
Hägele, G. F., Díaz, Á. I., Terlevich, E., et al. 2008, MNRAS, 383, 209
Hidalgo, S. L., Aparicio, A., Skillman, E., et al. 2011, ApJ, 730, 14
Immeli, A., Samland, M., Westera, P., & Gerhard, O. 2004, ApJ, 611, 20
Izotov, Y. I., Guseva, N. G., & Thuan, T. X. 2011, ApJ, 728, 161
Kennicutt, Jr., R. C. 1998, ARA&A, 36, 189
Kingdon, J. B. & Ferland, G. J. 1998, ApJ, 506, 323
Kingsburgh, R. L. & Barlow, M. J. 1994, MNRAS, 271, 257
Koleva, M., Bouchard, A., Prugniel, P., De Rijcke, S., & Vauglin, I. 2013, MNRAS, 428, 2949
Köppen, J. & Hensler, G. 2005, A&A, 434, 531
Kunth, D. & Östlin, G. 2000, A&A Rev., 10, 1
Lara-López, M. A., Cepa, J., Bongiovanni, A., et al. 2010, A&A, 521, L53
Lebouteiller, V., Heap, S., Hubeny, I., & Kunth, D. 2013, A&A, 553, A16
Lee, H., Bell, E. F., & Somerville, R. S. 2008, in IAU Symposium, Vol. 255, IAU Symposium, ed. L. K. Hunt, S. C. Madden, & R. Schneider, 100–105
Lelli, F., Verheijen, M., Fraternali, F., & Sancisi, R. 2012, A&A, 537, A72
Levesque, E. M., Berger, E., Soderberg, A. M., & Chornock, R. 2011, ApJ, 739, 23
Li, Y., Bresolin, F., & Kennicutt, Jr., R. C. 2013, ApJ, 766, 17
López-Sánchez, Á. R., Koribalski, B. S., van Eymeren, J., et al. 2012, MNRAS, 419, 1051
Mac Low, M.-M. & Ferrara, A. 1999, ApJ, 513, 142
Mannucci, F., Cresci, G., Maiolino, R., Marconi, A., & Gnerucci, A. 2010, MNRAS, 408, 2115
McGaugh, S. S. 1991, ApJ, 380, 140
Miyauchi-Isobe, N., Maehara, H., & Nakajima, K. 2010, Publications of the National Astronomical Observatory of Japan, 13, 9
Morales-Luis, A. B., Sánchez Almeida, J., Aguerri, J. A. L., & Muñoz-Tuñón, C. 2011, ApJ, 743, 77
Moran, S. M., Heckman, T. M., Kauffmann, G., et al. 2012, ApJ, 745, 66
Noguchi, M. 1999, ApJ, 514, 77
Papaderos, P., Guseva, N. G., Izotov, Y. I., & Fricke, K. J. 2008, A&A, 491, 113
Papaderos, P., Loose, H.-H., Thuan, T. X., & Fricke, K. J. 1996, A&AS, 120, 207
Peimbert, M. 1967, ApJ, 150, 825
Peimbert, M. & Costero, R. 1969, Boletin de los Observatorios Tonantzintla y Tacubaya, 5, 3
Pérez-Montero, E. & Contini, T. 2009, MNRAS, 398, 949
Pérez-Montero, E., Contini, T., Lamareille, F., et al. 2013, A&A, 549, A25
Pérez-Montero, E. & Díaz, A. I. 2003, MNRAS, 346, 105
Pettini, M. & Pagel, B. E. J. 2004, MNRAS, 348, L59
Queyrel, J., Contini, T., Kissler-Patig, M., et al. 2012, A&A, 539, A93
Reichard, T. A., Heckman, T. M., Rudnick, G., et al. 2009, ApJ, 691, 1005
Roy, J.-R. & Kunth, D. 1995, A&A, 294, 432
Sánchez Almeida, J., Aguerri, J. A. L., & Muñoz-Tuñón, C. 2013a, in Revista Mexicana de Astronomia y Astrofisica, vol. 27, Vol. 42, Revista Mexicana de Astronomia y Astrofisica Conference Series, 111–111
Sánchez Almeida, J., Aguerri, J. A. L., Muñoz-Tuñón, C., & Vazdekis, A. 2009, ApJ, 698, 1497
Sánchez Almeida, J., Muñoz-Tuñón, C., Amorín, R., et al. 2008, ApJ, 685, 194
Sánchez Almeida, J., Muñoz-Tuñón, C., Elmegreen, D. M., Elmegreen, B. G., & Méndez-Abreu, J. 2013b, ApJ, 767, 74
Sánchez Almeida, J., Terlevich, R., Terlevich, E., Cid Fernandes, R., & Morales-Luis, A. B. 2012, ApJ, 756, 163
Shaw, R. A. & Dufour, R. J. 1995, PASP, 107, 896
Shi, F., Kong, X., Li, C., & Cheng, F. Z. 2005, A&A, 437, 849
Silk, J. & Mamon, G. A. 2012, Research in Astronomy and Astrophysics, 12, 917
Skillman, E. D., Kennicutt, R. C., & Hodge, P. W. 1989, ApJ, 347, 875
Stasińska, G. 2004, in Cosmochemistry. The melting pot of the elements, ed. C. Esteban, R. García López, A. Herrero, & F. Sánchez, 115–170
Stasińska, G. 2010, in IAU Symposium, Vol. 262, IAU Symposium, ed. G. R. Bruzual & S. Charlot, 93–96
Stasińska, G., Morisset, C., Simón-Díaz, S., et al. 2013, A&A, 551, A82
Stasińska, G., Prantzos, N., Meynet, G., et al. 2012, in EAS Publications Series, Vol. 54, EAS Publications Series, ed. G. Stasińska, N. Prantzos, G. Meynet, S. Simón-Díaz, C. Chiappini, M. Dessauges-Zavadsky, C. Charbonnel, H.-G. Ludwig, C. Mendoza, N. Grevesse, M. Arnould, B. Barbuy, Y. Lebreton, A. Decourchelle, V. Hill, P. Ferrando, G. Hébrard, F. Durret, M. Katsuma, & C. J. Zeippen, 3–63
Stasińska, G. & Szczerba, R. 2001, A&A, 379, 1024
Stoughton, C., Lupton, R. H., Bernardi, M., et al. 2002, AJ, 123, 485
Straughn, A. N., Cohen, S. H., Ryan, R. E., et al. 2006, ApJ, 639, 724
Tenorio-Tagle, G. 1996, AJ, 111, 1641
Torres-Peimbert, S. & Peimbert, M. 2003, in IAU Symposium, Vol. 209, Planetary Nebulae: Their Evolution and Role in the Universe, ed. S. Kwok, M. Dopita, & R. Sutherland, 363
Tremonti, C. A., Heckman, T. M., Kauffmann, G., et al. 2004, ApJ, 613, 898
van der Kruit, P. C. & Freeman, K. C. 2011, ARA&A, 49, 301
Vilchez, J. M., Pagel, B. E. J., Diaz, A. I., Terlevich, E., & Edmunds, M. G. 1988, MNRAS, 235, 633
Werk, J. K., Putman, M. E., Meurer, G. R., et al. 2010, ApJ, 715, 656
Wilcots, E. M. & Miller, B. W. 1998, AJ, 116, 2363
Windhorst, R. A., Cohen, S. H., Straughn, A. N., et al. 2006, New Astron. Rev., 50, 821
Yates, R. M., Kauffmann, G., & Guo, Q. 2012, MNRAS, 422, 215
Zahid, H. J., Kashino, D., Silverman, J. D., et al. 2013, ArXiv e-prints